Correspondence

Estimation of Ultrasound Attenuation from Broadband Echo-Signals Using Bandpass Filtering

Hyungsuk Kim, James A. Zagzebski, and Tomy Varghese

***Abstract*—A problem with video signal analysis for estimating frequency-dependent ultrasonic attenuation is that relative echogenicity versus depth curves are distorted when broadband pulses are used. In this correspondence, we present results that demonstrate improved accuracy of attenuation estimates computed from B-mode or envelope data derived after narrowband (1 MHz BW) filtering at different frequencies around the center frequency of the broadband echo signal. Based on the premise that transducer center frequencies are selected in part on penetration or imaging depth requirements, simulation and experimental results for a typical ultrasound imaging system show that narrowband video signal analysis for frequencies lower than or at the center frequency of the broadband pulse provide unbiased attenuation estimation over this depth. Filtered signals above the center frequency of the pulse yield accurate results only at shallow depths.**

I. Introduction

Attenuation estimations in soft tissue with ultrasound pulse-echo systems are of interest because ultrasonic attenuation is intrinsically related to pathological changes in tissue [1], [2]. Measurements of ultrasonic attenuation have been helpful in identifying diffuse liver disease and benign conditions in the breast [3], [4]. However, time-gain compensation (TGC) and artifacts due to shadowing or enhancement of the ultrasound signals below higher or lower attenuating regions introduce difficulties in the interpretation of B-mode images. Accurate estimation of ultrasound attenuation in soft tissue, therefore, can not only provide useful diagnostic information but also could enable clear interpretation of B-mode images.

Attenuation estimation methods can be classified as either time or frequency-domain approaches [5], [6]. Most frequency-domain methods use either the spectral difference [7] or the spectral shift of the centroid of the echo signal power spectra [8] versus depth along the beam propagation direction. Among time-domain approaches, Flax *et al.* [9] proposed measurement of the zero crossing density of RF echo signals, the counterpart of spectral shift methods in the frequency domain. He and Greenleaf utilized the local maximum of the RF echo signal envelope for attenuation estimation [10], while Jang *et al.* [11] measured attenuation using the entropy difference between two adjacent segments of narrowband RF echo signals. Video or B-mode signal analysis methods were developed by Knipp *et al.* [12] to estimate attenuation directly from B-mode images.

Time-domain methods are easier to implement and computationally faster. However, it is difficult to compensate for local variations in the sound field along the beam propagation direction (i.e., diffraction effects). The video signal analysis (VSA) method [12] computes ratios of the mean echo signal intensity from a sample to that from a reference phantom scanned using identical ultrasound system settings. Thus, this method effectively compensates for diffraction effects, enabling real-time application in a clinical environment. However, relative intensity versus depth curves that yield information on the attenuation of the sample become progressively distorted as the bandwidth of the transmit pulse increases, particularly at deeper depths in tissue.

In this correspondence, we investigate the estimation accuracy of attenuation coefficients computed using the VSA method after bandpass filtering of the RF signal prior to forming B-mode images. Echo signals characteristic of a typical ultrasound system are simulated, and narrowband Chebyshev-II filters centered at different frequencies around the center frequency of the broadband transmit pulse are used to filter the RF data. B-mode signals derived from the filtered data are processed to estimate attenuation coefficients. Simulation and experimental results with a uniformly attenuating tissue-mimicking (TM) phantom were used to determine the accuracy of this approach. Depth settings over which data are analyzed are consistent with the penetration distance for the chosen ultrasound frequency.

In Section II, a brief derivation of the VSA method is presented. An ultrasound simulation program and methods for estimating the attenuation coefficient using a narrowband filtering technique are presented in Section III. Simulation results that illustrate the use of bandpass filtering to obtain unbiased results using lower frequency components also are described in Section III. In Section IV, experimental results using TM phantom data are presented.

II. Video Signal Analysis Method

Most methods that estimate the attenuation coefficient using pulse-echo data assume a linear frequency dependence of the attenuation, uniform backscatter, and constant speed of sound in the region of interest (ROI). Other assumptions include weak scattering, namely that contributions due to multiple scattering can be ignored (i.e., the Born approximation). Under these assumptions, the

Manuscript received August 28, 2007; accepted December 16, 2007.

The authors are with the University of Wisconsin-Madison, Medical Physics, Madison, WI (e-mail: hyungsuk@cae.wisc.edu).

H. Kim is also with the University of Wisconsin-Madison, Electrical and Computer Engineering, Madison, WI.

Digital Object Identifier 10.1109/TUFFC.2008.768

intensity of the backscattered RF signal received at the ultrasound transducer, $R(f,z)$, can be expressed in the frequency domain as a product of the transmit pulse, diffraction, attenuation, and backscatter terms:

$$R(f,z) = G(f) \cdot D(f,z) \cdot A(f,z) \cdot B(f), \tag{1}$$

where z denotes the depth from the transducer, $G(f)$ represents the combined effect of the transmit pulse and transducer sensitivity (force-to-voltage transfer function) during reception, which depends on transducer design and the transmitted pulse, $D(f,z)$ denotes diffraction effects related to transducer parameters that include focusing, and $A(f,z)$ represents cumulative attenuation in soft tissue. Attenuation is assumed to be linearly proportional to frequency [13] and is given by:

$$A(f,z) = \exp(-4\beta f z), \tag{2}$$

where β is the slope of the attenuation coefficient versus frequency, in units of Nepers/cm/MHz. Tissue backscatter, $B(f)$, is generally modeled as a power of frequency [14], [15].

$$B(f) = B_o f^n, \tag{3}$$

where B_o is a constant. The parameter n can vary from 0 for specular reflection to 4 for Rayleigh scattering.

Computing the ratio of the intensity of the backscattered RF signals from the sample to that from a reference phantom recorded using identical transducer and system settings was previously used to eliminate the transducer-dependent terms, $G(f)$ and $D(f,z)$. Thus, the ratio of the intensities of the echo signals at depth z from a sample to those from a reference phantom at the same depth is expressed as [16]:

$$RS(f,z) = \frac{B_s(f)}{B_r(f)} \cdot \exp\{-4(\beta_s - \beta_r) f\, z\}, \tag{4}$$

where the subscripts r and s represent the reference and sample, respectively.

Using the VSA method, the ratio of intensities of backscattered RF signals is approximated by the ratio of the signals derived from B-mode images. Assuming that the backscattered signal frequency bandwidth contributing to the B-mode image data is not broadband, we can approximate $\sqrt{RS(f,z)}$ in (4) with the ratio of average signal amplitudes for the reference and sample at depth z [12] as:

$$RE(z) = \frac{E_s(z)}{E_r(z)} = \sqrt{\frac{B_s(f_{\text{eff}})}{B_r(f_{\text{eff}})} \cdot \exp\{-4(\beta_s - \beta_r)\, f_{\text{eff}}\, z\}}, \tag{5}$$

where $E_r(z)$ and $E_s(z)$ represent the average signal amplitude from the reference and sample at depth z, and f_{eff} represents an "effective frequency," defined as the ultrasound frequency that yields the same value of backscatter and attenuation in the sample as the B-mode signal. Under the assumption of linear frequency dependence of attenuation, the difference between attenuation coefficients versus frequency slopes of the reference and sample after linear regression over the beam propagation direction is given by:

$$\Delta\beta(\text{dB/cm/MHz}) = -\frac{8.686}{2f_{\text{eff}}} \cdot \frac{d\log(RE(z))}{dz}. \tag{6}$$

Because the attenuation coefficient of the reference is known, that of the sample can be estimated using (6).

III. VSA Simulations

A. Ultrasound Simulation Procedure

RF echo signals for both reference and sample phantoms with various values of attenuation coefficient were simulated. The simulation program is based on classical diffraction theory for continuous wave propagation [17] and accurately computes pulsed transmit-receive beam patterns using superposition. For this study, a linear-array transducer consisting of rectangular elements of size 0.2 mm by 10 mm, with a center-to-center separation of 0.2 mm was modeled. Each beam line formed by the array used up to 128 consecutive elements. Dynamic receive focusing and dynamic aperture were used such that the receive F-number was fixed at 2. The ultrasound field varies with axial distance from the transducer. A Gaussian-shaped pulse with a center frequency of 5 MHz was simulated for the received pulse at the surface of the sample. The bandwidth of the pulse was set to 80%, unless otherwise specified. Changes in the signal spectrum with depth are accounted for in the beam model, in which a complex wave number is used to introduce specific values for both speed of sound and medium attenuation.

Two numerical, uniform phantoms were simulated by assuming a random distribution of 25 μm glass beads in media having a sound speed of 1540 m/s. The scatterer number density was set at 9.7 per cubic millimeter, which yields Rayleigh statistics [18]. The modeled phantom dimensions were 40 mm (width) by 80 mm (height) by 10 mm (thickness), thus requiring 3.1×10^5 scatterers in the model. The distance between adjacent beam lines was set to 0.2 mm, the same as the element pitch. The transducer was assumed to be in direct contact with the sample or reference phantom, and the axial transmit focus as well as the elevational focus were both set to 40 mm. Simulations were performed over a 1–15 MHz frequency range, with a 0.1 MHz increment between frequency components. The backscattered signals were computed by first applying a Gaussian filter centered at 5 MHz with the specified frequency bandwidth of the transducer, then computing the inverse Fourier transform. This yielded RF echo data for each beam line used to form the simulated ultrasound images.

After generating simulated RF data with a specified value of the attenuation coefficient, echo signal envelopes were obtained by computing the analytic signal using

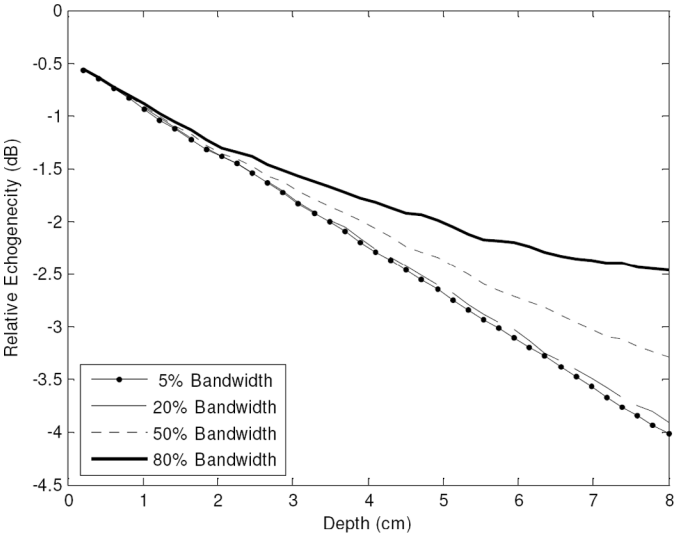

Fig. 1. Logarithm of the relative echogenicity versus depth for a simulated, uniformly attenuating phantom for various transmit-receive pulse bandwidths. The attenuation coefficients of the reference and sample are 0.3 dB/cm/MHz and 0.7 dB/cm/MHz, respectively.

the Hilbert transform, and then taking its magnitude. The envelope echo data frame was then subdivided into small, overlapping two-dimensional (2-D) blocks to compute mean echo intensities over each block. Typical block sizes were 2 mm by 2 mm. The intensity value was divided by corresponding values from the reference phantom, to yield the echogenicity of the block relative to that from the reference at the same depth. A 50% overlap of each 2-D block was used along both axial and lateral directions to obtain additional relative echogenicity versus depth profiles for the simulated data. Attenuation estimates were then computed using a linear regression over 15 of the 2-mm by 2-mm blocks along the axial direction corresponding to a 16-mm data segment for 50% overlap of the blocks. These processing parameters are used throughout the correspondence.

B. Simulation Results

As previously reported by Tu *et al.* [19], the logarithm of the relative echogenicity versus depth is a straight line whose instantaneous slope depends on the difference between the attenuation coefficients of the sample and reference at the corresponding depth. Tu *et al.* also pointed out that, for broadband data, this line becomes a curve for which the departure from a straight line depends on the bandwidth of the echo signal and the difference between the sample and reference attenuation coefficients. Fig. 1 plots the logarithm of the relative echogenicity versus depth for simulated data from a phantom with a uniform attenuation value. Four different ultrasound pulse bandwidths (i.e., 5%, 20%, 50%, and 80%) were simulated for Fig. 1. The attenuation coefficients of the reference and sample were 0.3 dB/cm/MHz and 0.7 dB/cm/MHz, respectively. For a narrow bandwidth, the logarithm of the relative echogenicity versus depth is a straight line. However, as the bandwidth of the pulse increases, the logarithm of this ratio deviates from a straight line because of varying frequency-dependent attenuation in the sample and reference. This phenomenon is clearly visualized at deeper depths.

Typical imaging systems use frequency bandwidths of 60% or greater. The broadband RF echo signal itself can be filtered to enable accurate estimation of the attenuation coefficient. Here an 80% bandwidth signal was decomposed into multiple narrowband signals using bandpass filtering. Filter center frequencies were selected to lie on either side of the 5 MHz center frequency of the original broadband echo signal, and the bandwidth was set to 1 MHz. Bandpass filters centered at 3, 4, 5, 6, and 7 MHz were applied. Each bandpass filtered RF signal then was processed using the VSA method to investigate the estimation accuracy.

C. Results for Bandpass Filtering

The logarithm of the relative echogenicity versus depth of the broadband RF data and the bandpass filtered signals are shown in Fig. 2(a). The relative echogenicity of the bandpass filtered RF signals, particularly those at lower frequencies, exhibit a nearly linear decrease with depth. The echogenicity ratio versus depth at higher filter frequencies, however, still deviates from a straight line at deeper depths. Evidently, a narrower filter bandwidth would have to be used for these relative attenuation values to accurately determine attenuation at deeper depths. Fig. 2(b) shows the estimated sample attenuation coefficient values versus depth, computed from local values of the slopes of the curves in Fig. 2(a). Notice that the attenuation coefficient derived from the bandpass filtered signals obtained for the higher filter center frequencies, as well as from the original broadband pulse, underestimate the actual attenuation coefficient value (0.7 dB/cm/MHz), particularly at deeper propagation depths. Based on our simulation results, the filtered signals at or below the center frequency of the transmitted ultrasound pulse would provide the best attenuation coefficient results.

We derived "attenuation coefficient images" of the simulated sample phantom using the same processing parameters. To form an image, mean pixel values were computed over 2 mm × 2 mm sized blocks, and a 16 mm linear regression window applied along the axial direction. Attenuation values computed in this manner over the entire imaged region are represented in grayscale. Examples are shown in Fig. 3. Because the relative echogenicity curves are distorted at deeper depths, attenuation coefficient values of the sample derived with the broadband signal, shown in Fig. 3(a), are likewise underestimated at deeper depths. However, the bandpass filtered signals at frequencies below the center frequency of the 5-MHz pulse, shown in Fig. 3(b) and (c), provide unbiased estimations over the entire depth range considered here. Bandpass filtered signals at higher center frequencies, shown in Fig. 3(d), provide meaningful attenuation estimation results, but only at shallow depths.

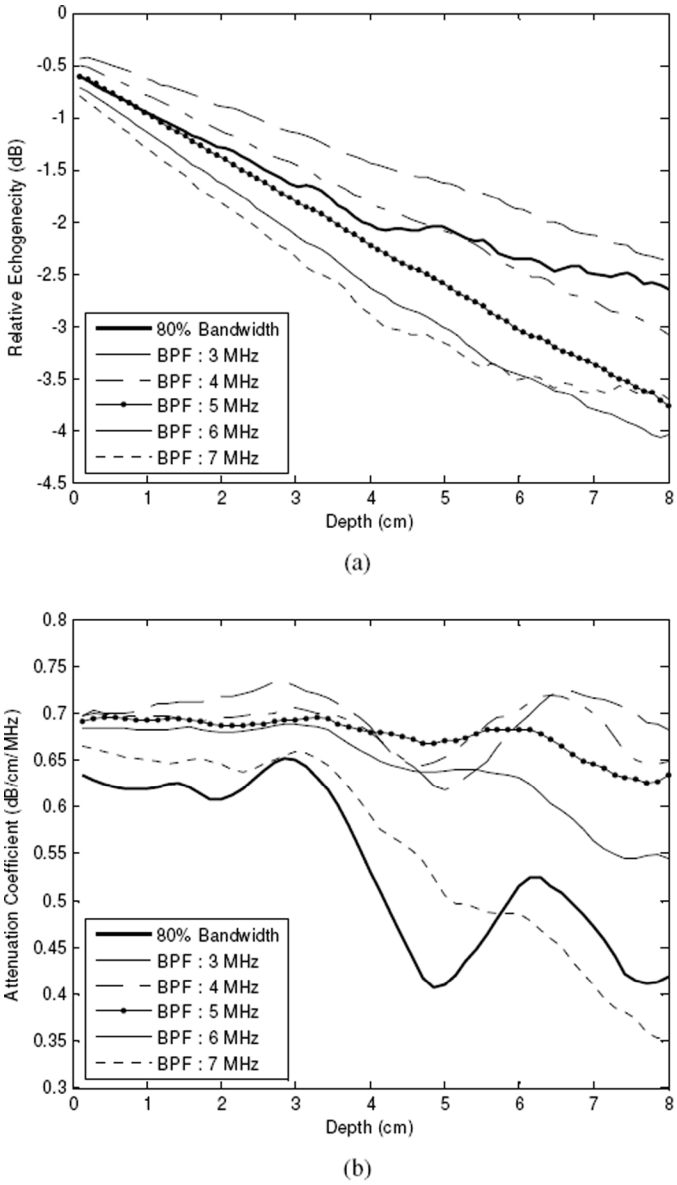

Fig. 2. Simulation results from a uniform attenuation phantom. The relative echogenicity between the sample and reference as derived from the original broadband signal and after bandpass filtering signals are plotted as a function of depth. The attenuation coefficients of the reference and sample are 0.3 dB/cm/MHz and 0.7 dB/cm/MHz, respectively. (a) The logarithm of the relative echogenicity versus depth. (b) The estimated attenuation coefficients of the sample.

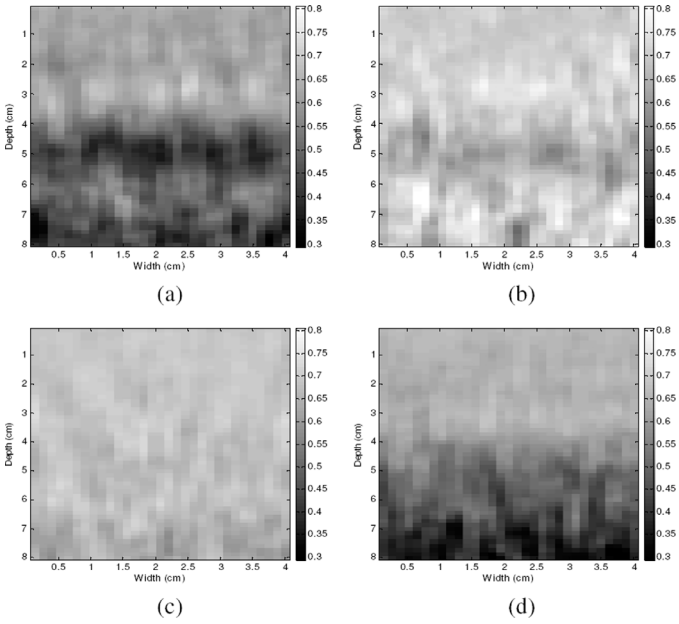

Fig. 3. Attenuation coefficient images for the simulated, uniform phantom. Attenuation coefficients of the reference and sample were 0.3 dB/cm/MHz and 0.7 dB/cm/MHz, respectively. (a) Broadband pulse data. (b) Bandpass filtered at 3 MHz. (c) Bandpass filtered at 5 MHz. (d) Bandpass filtered at 7 MHz.

As previously reported by Tu *et al.* [19], VSA accurately estimates the attenuation coefficient when the attenuation coefficient of the reference is close to that of the sample. We also investigate the estimation performance of the bandpass filtering technique with increasing attenuation coefficient differences between the reference and sample. The attenuation coefficient of the simulated reference phantom was increased from 0.1 dB/cm/MHz to 0.9 dB/cm/MHz; that of the sample was maintained at 0.5 dB/cm/MHz. The attenuation coefficients estimated were averaged over a depth of 2–4 cm to obtain the mean and variance. Fig. 4 presents results obtained after bandpass filtering at the center frequency (5 MHz) of the original data as well as at the lower and upper ends of the spectrum (3 MHz and 7 MHz), respectively. The VSA method using narrowband filtering underestimates the attenuation coefficient when the attenuation coefficient of the reference is lower than that of the sample. However, when the attenuation coefficient of the reference is larger than that of the sample, it overestimates the value of the sample attenuation coefficient. The variance among attenuation estimations over the 2–4 cm depth range also become larger as the difference between the attenuation coefficient of the reference and sample increases as shown in Fig. 4.

IV. Experimental Results

In addition to the numerical phantom data, two TM phantoms manufactured in our laboratory were used to evaluate the performance of the bandpass filtered VSA method. The first was a quality assurance phantom, referred to as the "Gammex/RMI 409 ACR Prototype," having two sections with different attenuation coefficients. A section with an attenuation coefficient of 0.5 dB/cm/MHz was used as the reference, and a section with 0.7 dB/cm/MHz attenuation was used as the sample. A second TM phantom, referred to as the "attenuation phantom" (AP), contains a cylindrical inclusion with an attenuation coefficient of 0.8 dB/cm/MHz, embedded in a background that has an attenuation of 0.5 dB/cm/MHz. Both background and inclusion have the same concentration of 20 μm glass beads [20] that provide scattering. To acquire reference RF signals for the experiment, a uniformly attenuating TM phantom was used, having an attenuation coefficient of 0.5 dB/cm/MHz [21].

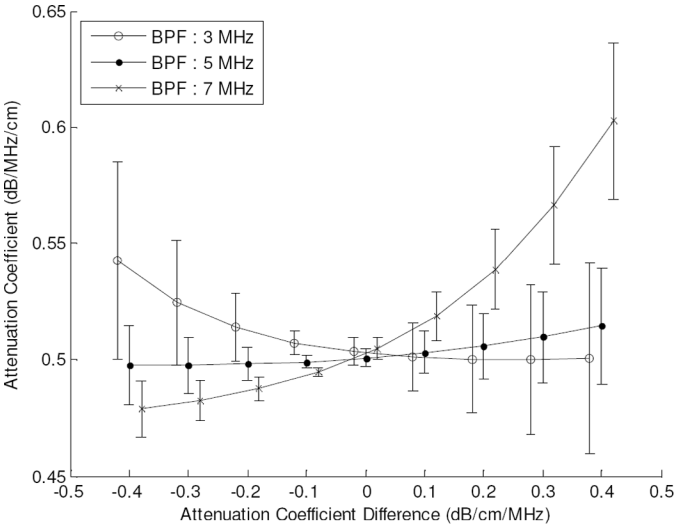

Fig. 4. Estimated attenuation coefficients for a 0.5 dB/cm/MHz sample using different values of the attenuation coefficient for the reference phantom. The x-axis represents the difference between the attenuation coefficients of the reference and sample. The errorbars denote the estimation variances. The transmit pulse has a 5 MHz center frequency with 80% bandwidth, and narrow bandpass filtering is applied at 3, 5, and 7 MHz.

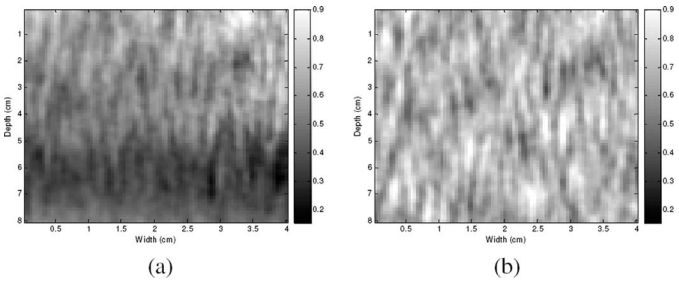

Fig. 5. Attenuation coefficient images for the Gammex/RMI prototype phantom. Each pixel in the image represents an estimated attenuation coefficient. The attenuation coefficient of the reference and sample are 0.5 dB/cm/MHz and 0.7 dB/cm/MHz, respectively. (a) Broadband pulse data. (b) Bandpass filtered at 4 and 5 MHz with frequency compounding.

The phantoms were scanned using a Siemens Antares ultrasound system (Siemens Medical Systems, Issaquah, WA) using a linear array transducer (VFX 9-5) with a 5 MHz center frequency and 80% bandwidth. RF data digitized at a 40 MHz sampling frequency were acquired using the Siemens Axius Direct Ultrasound Research Interface, and narrowband filtering was performed offline on the broadband data. The VSA method then was applied to the envelope data computed using a Hilbert transform.

An attenuation coefficient image of the Gammex/RMI 409 ACR Prototype (Gammex RMI, Middleton, WI) is shown in Fig. 5. The VSA method using broadband signals underestimates the attenuation coefficient, especially at deeper depths shown in Fig. 5(a). Filter center frequencies of 4 and 5 MHz then were used to obtain narrowband RF signals. Fig. 5(b) shows an attenuation coefficient image obtained by averaging attenuation coefficient estimates at these two frequencies, i.e., applying frequency compounding [22].

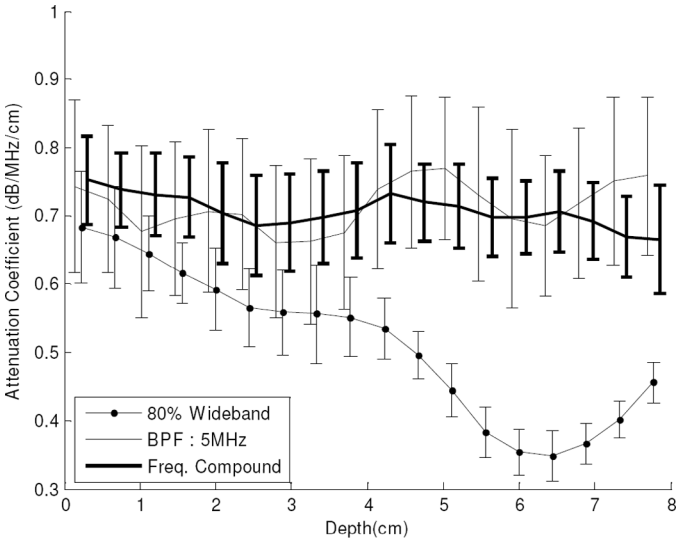

Fig. 6. Experimental results obtained from a uniform attenuation phantom. The original broadband signal and narrow bandpass filtered signals are plotted as a function of depth. The attenuation coefficients of the reference and sample are 0.5 dB/cm/MHz and 0.7 dB/cm/MHz, respectively.

Fig. 6 shows the estimated values of the attenuation coefficients obtained for the same TM phantom along the beam propagation direction. Although the VSA method using broadband pulses underestimates the attenuation coefficient for increasing propagation depths, VSA used after bandpass filtering provides unbiased values that are independent of depth. The estimation variance with the single narrowband filtered signal is larger than that obtained using the entire broadband pulse data because the narrowband filtered RF signals contains less information than broadband signals. However, after frequency compounding, the estimation variances are reduced and are comparable to results obtained using the original broadband data.

Experimental results obtained using the inclusion phantom (AP) is shown in Fig. 7. On a B-mode image [Fig. 7(a)], the 3 cm diameter inclusion is seen because of faint specular echoes (arrow) from the proximal and distal surfaces as well as from the acoustical shadow. An attenuation image after applying VSA processing on broadband data is presented in Fig. 7(b), and one using VSA on filtered data is shown in Fig. 7(c). Attenuation estimates for a ROI consisting of a circle whose diameter is one-half that of the projected area of the inclusion were 0.64 dB/cm/MHz for image data in Fig. 7(b) and 0.78 dB/cm/MHz for that in Fig. 7(c). Although VSA using broadband data underestimates the attenuation coefficient value, VSA using bandpass filtered data, and frequency compounding provides an accurate estimate of the attenuation coefficient of the ROI.

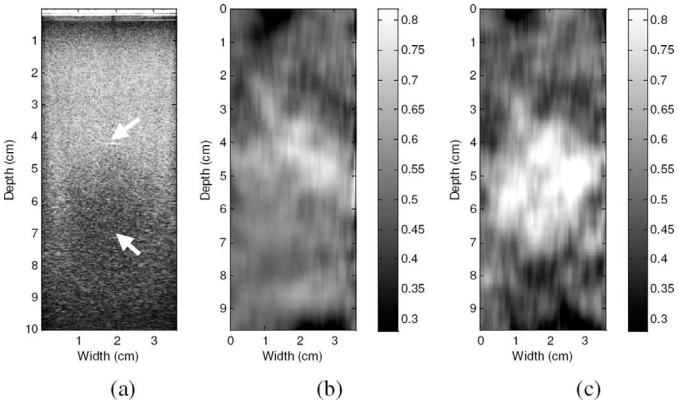

Fig. 7. B-mode image and attenuation coefficient images of a TM phantom containing a cylindrical inclusion whose attenuation coefficient is 0.8 dB/cm/MHz in a background whose attenuation is 0.5 dB/cm/MHz. Each pixel in the image represents an estimated value of the attenuation coefficient. (a) B-mode image of a sample phantom. (b) Broadband pulse data. (c) Bandpass filtered at 4 and 5 MHz with frequency compounding.

V. Discussion

Although the VSA method directly computes the attenuation coefficient from envelope or B-mode signals and has improved computational efficiency for real-time application, broadband transmit pulses used in current ultrasound pulse-echo systems result in distortion of relative echogenicity versus depth data. The use of narrowband filtering, however, can provide unbiased estimation of the attenuation properties while maintaining the computational efficiency of the VSA method. Such filtered signals could readily be provided as adjunct data in modern, software-based ultrasound machines.

Based on our results, filtered RF signals, lower than or at the center frequency of the original broadband pulse, provide the best attenuation results at large depths. Because higher frequency components attenuate faster than lower ones, filtered signals at lower frequencies maintain relatively useful frequency information from the backscattered echo signals.

Because narrower bandwidth filters use only small portions of frequency information present in the broadband RF signals, the estimated attenuation coefficients have larger estimation variances and were underestimated at deeper depths in our experiments. However, for broader bandwidth filters, estimated results indicate similar behavior as the broadband pulse case. Based on our simulation and experimental results, the 1 MHz bandwidth filter provides relatively stable estimation performance independent of depth, with smaller estimation variances than other narrower/broader bandwidth filters.

The relative difference between attenuation coefficients of the reference and sample also influence the estimation performance of the VSA method. A smaller attenuation difference provides more accurate estimations with better estimation precision. Because the attenuation properties of the sample are unknown, multiple reference phantoms with different attenuation coefficient values may improve the estimation performance by matching the attenuation properties of the sample.

VI. Conclusions

We investigated the accuracy of VSA attenuation estimates computed from B-mode images obtained after bandpass filtering of the broadband echo signals. Over the penetration range associated with the transducer center-frequency setting, simulation and experimental results show that local attenuation coefficient estimates obtained using the filtered envelope data demonstrate comparable results to other existing estimation methods. Caution must be exercised, however, when applying the VSA analysis to frequency components above the center frequency, as accurate results for these signals were only obtained for shallow depths. Errors in applying the VSA method worsen if the attenuation coefficient of the reference is significantly different from that of the sample.

References

[1] M. J. Cloostermans and J. M. Thijssen, "A beam corrected estimation of the frequency dependent attenuation of biological tissues from backscattered ultrasound," *Ultrason. Imag.*, vol. 5, no. 2, pp. 136–147, 1983.

[2] P. A. Narayana and J. Ophir, "On the frequency dependence of attenuation in normal and fatty liver," *IEEE Trans. Sonics Ultrason.*, vol. 30, no. 6, pp. 379–383, 1983.

[3] G. Berger, P. Laugier, J. C. Thalabard, and J. Perrin, "Global breast attenuation: Control group and benign breast diseases," *Ultrason. Imag.*, vol. 12, no. 1, pp. 47–57, 1990.

[4] B. J. Oosterveld, J. M. Thijssen, P. C. Hartman, R. L. Romijn, and G. J. Rosenbusch, "Ultrasound attenuation and texture analysis of diffuse liver disease: Methods and preliminary results," *Phys. Med. Biol.*, vol. 36, no. 8, pp. 1039–1064, 1991.

[5] E. Walach, A. Shmulewitz, Y. Itzchak, and Z. Heyman, "Local tissue attenuation images based on pulse-echo ultrasound scans," *IEEE Trans. Biomed. Eng.*, vol. 36, pp. 211–221, 1989.

[6] M. Fink, F. Hottier, and J. F. Cardoso, "Ultrasonic signal processing for in vivo attenuation measurement: Short time Fourier analysis," *Ultrason. Imag.*, vol. 5, no. 2, pp. 117–135, 1983.

[7] B. Zhao, O. A. Basir, and G. S. Mittal, "Estimation of ultrasound attenuation and dispersion using short time Fourier transform," *Ultrasonics*, vol. 43, pp. 375–381, 2004.

[8] R. Kuc and H. Li, "Reduced-order autoregressive modeling for center-frequency estimation," *Ultrason. Imag.*, vol. 7, no. 3, pp. 244–251, 1985.

[9] S. W. Flax, N. J. Pelc, G. H. Glover, F. D. Gutmann, and M. McLachlan, "Spectral characterization and attenuation measurements in ultrasound," *Ultrason. Imag.*, vol. 5, no. 2, pp. 95–116, 1983.

[10] P. He and J. F. Greenleaf, "Application of stochastic-analysis to ultrasonic echoes—estimation of attenuation and tissue heterogeneity from peaks of echo envelope," *J. Acoust. Soc. Amer.*, vol. 79, no. 2, pp. 526–534, 1986.

[11] H. S. Jang, T. K. Song, and S. B. Park, "Ultrasound attenuation estimation in soft tissue using the entropy difference of pulsed echoes between two adjacent envelope segments," *Ultrason. Imag.*, vol. 10, no. 4, pp. 248–264, 1988.

[12] B. S. Knipp, J. A. Zagzebski, T. A. Wilson, F. Dong, and E. L. Madsen, "Attenuation and backscatter estimation using video signal analysis applied to B-mode images," *Ultrason. Imag.*, vol. 19, no. 3, pp. 221–233, 1997.

[13] R. Kuc, "Bounds on estimating the acoustic attenuation of small tissue regions from reflected ultrasound," *Proc. IEEE*, vol. 73, no. 7, pp. 1159–1168, 1985.

[14] K. K. Shung, R. A. Sigelmann, and J. M. Reid, "Scattering of ultrasound by blood," *IEEE Trans. Biomed. Eng.*, vol. 23, pp. 460–467, 1976.

[15] K. A. Wear, B. S. Garra, and T. J. Hall, "Measurements of ultrasonic backscatter coefficients in human liver and kidney in vivo," *J. Acoust. Soc. Amer.*, vol. 98, pp. 1852–1857, 1995.

[16] L. X. Yao, J. A. Zagzebski, and E. L. Madsen, "Backscatter coefficient measurements using a reference phantom to extract depth-dependent instrumentation factors," *Ultrason. Imag.*, vol. 12, no. 1, pp. 58–70, 1990.

[17] Y. Li and J. A. Zagzebski, "A frequency domain model for generating B-mode images with array transducers," *IEEE Trans. Ultrason., Ferroelect., Freq. Contr.*, vol. 46, no. 3, pp. 690–699, 1999.

[18] R. F. Wagner, S. W. Smith, J. M. Sandrick, and H. Lopez, "Statistics of speckle in ultrasound B-scans," *IEEE Trans. Sonics Ultrason.*, vol. 30, pp. 156–163, 1983.

[19] H. Tu, J. A. Zagzebski, and Q. Chen, "Attenuation estimations using envelope echo data: Analysis and simulations," *Ultrasound Med. Biol.*, vol. 32, no. 3, pp. 377–386, 2006.

[20] H. Tu, "Ultrasonic attenuation imaging and analysis," Ph.D. dissertation, Department of Medical Physics, University of Wisconsin-Madison, pp. 44–47, 2005.

[21] T. Wilson, J. Zagzebski, and Y. Li, "A test phantom for estimating changes in the effective frequency of an ultrasonic scanner," *J. Ultrasound Med.*, vol. 21, no. 9, pp. 937–945, 2002.

[22] H. Tu, J. A. Zagzebski, A. L. Gerig, Q. Chen, E. L. Madsen, and T. J. Hall, "Optimization of angular and frequency compounding in ultrasonic attenuation estimations," *J. Acoust. Soc. Amer.*, vol. 117, no. 5, pp. 3307–3318, 2005.